Title
In vivo directed differentiation of pluripotent stem cells for skeletal regeneration

Journal
Proceedings of the National Academy of Sciences of the United States of America, 109(50)

ISSN
0027-8424

Authors
Levi, Benjamin
Hyun, Jeong S
Montoro, Daniel T
et al.

Publication Date
2012-12-11

DOI
10.1073/pnas.1218052109

Peer reviewed

In vivo directed differentiation of pluripotent stem cells for skeletal regeneration

Benjamin Levi[a,1], Jeong S. Hyun[a,1], Daniel T. Montoro[a,1], David D. Lo[a], Charles K. F. Chan[b], Shijun Hu[c], Ning Sun[c], Min Lee[d], Monica Grova[a], Andrew J. Connolly[e], Joseph C. Wu[c], Geoffrey C. Gurtner[a], Irving L. Weissman[b,2], Derrick C. Wan[a,2], and Michael T. Longaker[a,b,2]

[a]Hagey Laboratory for Pediatric Regenerative Medicine, Department of Surgery, Plastic and Reconstructive Surgery Division, [c]Department of Medicine and Radiology, and [e]Department of Pathology, Stanford University School of Medicine, Stanford, CA 94305; [b]Institute for Stem Cell Biology and Regenerative Medicine, Stanford University, Stanford, CA 94305; and [d]Division of Advanced Prosthodontics, Biomaterials, and Hospital Dentistry, School of Dentistry, University of California, Los Angeles, CA 90095-1668

Contributed by Irving L. Weissman, October 17, 2012 (sent for review July 20, 2012)

Pluripotent cells represent a powerful tool for tissue regeneration, but their clinical utility is limited by their propensity to form teratomas. Little is known about their interaction with the surrounding niche following implantation and how this may be applied to promote survival and functional engraftment. In this study, we evaluated the ability of an osteogenic microniche consisting of a hydroxyapatite-coated, bone morphogenetic protein-2–releasing poly-L-lactic acid scaffold placed within the context of a macroenvironmental skeletal defect to guide in vivo differentiation of both embryonic and induced pluripotent stem cells. In this setting, we found de novo bone formation and participation by implanted cells in skeletal regeneration without the formation of a teratoma. This finding suggests that local cues from both the implanted scaffold/cell micro- and surrounding macroniche may act in concert to promote cellular survival and the in vivo acquisition of a terminal cell fate, thereby allowing for functional engraftment of pluripotent cells into regenerating tissue.

Pluripotent stem cells hold significant promise for the treatment of tissue deficiencies and other human diseases (1, 2). Both human induced pluripotent stem cells (h-iPSCs) and embryonic stem cells (h-ESCs) are capable of differentiating into a multitude of cell types from each of three germ layers, allowing investigators to devise novel platforms for research and therapeutic drug screening (3, 4). This same property has also made these cells a much more powerful tool compared with mesenchymal stromal cells for regenerative medicine. In addition, as h-iPSCs can be reprogrammed from a patient's own somatic cells, they have the added potential of mitigating some of the concerns over immunogenic sequelae that are raised with other cell types, yet simultaneously enabling development of patient-specific disease modeling (5–7).

Despite dramatic progress made over recent years, widespread application of pluripotent cells in clinical medicine has been hampered by several challenges, chief among which is the propensity for both h-iPSCs and h-ESCs to form tumors in vivo (8). As recent studies have shown development of teratomas to directly correlate with the number of residual undifferentiated cells implanted, several strategies have been proposed to eliminate these persistent pluripotent cells before injection (8–10). It is still unknown, however, if they can be completely successful in the context of the number of cells required for in vivo tissue regeneration. Furthermore, few reports have also demonstrated engraftment and functional integration of pluripotent cells into the surrounding tissue, and little is known about how transplanted cells truly interact with the endogenous niche following implantation. These niches may in fact play significant roles in stabilizing fully pluripotent cells and guiding acquisition of cell fate, while also minimizing teratoma formation (11).

In this study, we evaluated how a skeletal defect macroniche combined with a pro-osteogenic biomimetic scaffold microniche could provide cues affecting survival and differentiation of implanted cells lacking in a developmental program. In response to such an environment, not only did we find a high degree of survival, but the transplanted pluripotent cells were also shown to acquire a fully differentiated osteogenic state, integrating into the surrounding bone without the formation of a teratoma. Our data thus suggest that the surrounding niche is capable of not only supporting cellular viability, but can also guide differentiation of pluripotent cells for functional engraftment into regenerating tissue.

Results

In Vitro Differentiation of Pluripotent Cells. As bone morphogenetic proteins (BMPs) have been shown to both powerfully promote osteogenesis and regulate differentiation of pluripotent cells, the capacity for h-iPSCs and h-ESCs to respond to BMP-2 was first evaluated (12–14). At baseline, pSmad1/5 could not be detected in either type of pluripotent cell (Fig. S1 *A* and *D*). However, culturing h-iPSCs or h-ESCs with BMP-2 (200 ng/mL) resulted in increased levels of pSmad1/5, as demonstrated by Western blot analysis just 2 h following treatment. Importantly, this result was not accompanied by any appreciable change in baseline Smad5 levels (Fig. S1 *B* and *E*). Therefore, the canonical BMP signal transduction pathway is functionally active in both h-iPSCs and h-ESCs.

The effect of BMP-2 on pluripotency was next evaluated by culturing cells in growth medium, standard osteogenic differentiation medium (ODM), or ODM supplemented with BMP-2. After 3 d in ODM, 83.5% of cells were still found to be stage-specific embryonic antigen 4^+ (SSEA-4^+) (Fig. S1*G*, *Center*). In contrast, only 61.9% of cells were SSEA-4^+ when cultured with BMP-2 (Fig. S1*G*, *Right*). This result was associated with an increase in runt-related protein-2 (RUNX-2) expression, as 10.0% of cells in ODM were RUNX-2^+ but 31.4% of cells in ODM + BMP-2 were RUNX-2^+ (Fig. S1*H*, *Center* and *Right*, respectively). Therefore, treatment of pluripotent cells with BMP-2 accelerated acquisition of a more differentiated state.

To evaluate the ability to guide in vitro differentiation of pluripotent cells along an osteogenic lineage, h-iPSCs and h-ESCs were subsequently cultured in ODM supplemented with BMP-2. Immunostaining these cells for octamer-binding transcription factor 4 (OCT-4), NANOG, and SRY-related HMG-box (SOX)-2 after 7 d demonstrated reduction of expression for each of these pluripotent genes (Fig. 1 *A* and *B*) (15).

Author contributions: B.L., J.S.H., D.T.M., I.L.W., D.C.W., and M.T.L. designed research; B.L., J.S.H., D.T.M., D.D.L., C.K.F.C., M.G., and D.C.W. performed research; S.H., N.S., and M.L. contributed new reagents/analytic tools; B.L., J.S.H., D.T.M., D.D.L., C.K.F.C., A.J.C., J.C.W., G.C.G., I.L.W., D.C.W., and M.T.L. analyzed data; and B.L., J.S.H., D.T.M., I.L.W., D.C.W., and M.T.L. wrote the paper.

The authors declare no conflict of interest.

[1]B.L., J.S.H., and D.T.M. contributed equally to this work.

[2]To whom correspondence may be addressed. E-mail: irv@stanford.edu, dwan@stanford.edu, or longaker@stanford.edu.

This article contains supporting information online at www.pnas.org/lookup/suppl/doi:10.1073/pnas.1218052109/-/DCSupplemental.

Not surprisingly, concurrent up-regulation of osteogenic markers RUNX-2 and osteocalcin (OCN) was also appreciated among h-iPSCs and h-ESCs cultured in ODM with BMP-2 (Fig. 1 *C* and *D*) and Alizarin red staining revealed significantly greater extracellular matrix mineralization ($^*P < 0.05$) (Fig. 1 *E* and *F*). To confirm our histological staining, gene-expression analysis by quantitative real-time PCR was performed for RUNX-2 and OCN. At 7 d following culture in ODM with BMP-2, significantly increased levels of transcripts were noted for both of these genes ($^*P < 0.05$) (Fig. 1 *G* and *H*).

Osteogenic Microniche Promotes in Vivo Bone Regeneration. To demonstrate the baseline in vivo pluripotent capacity of our h-iPSC and h-ESC lines, kidney capsule injection of one-million pluripotent cells was performed in immunodeficient athymic mice (Fig. S2) (16). h-iPSCs were transduced with a firefly luciferase/red fluorescent protein/herpes simplex virus thymidine kinase triple-fusion reporter construct and h-ESCs were labeled with a firefly luciferase/green fluorescent protein construct to follow in vivo cell viability (17). With both cell types, there was a significant increase in luciferase imaging over time consistent with biologic activity and teratoma formation (Fig. S2*B*). Furthermore, tissue formation from all three embryonic germ layers could be readily observed histologically 8 wk following injection (Fig. S2*C*).

The ability for an increasingly osteogenic environment to guide in vivo differentiation of h-iPSCs and h-ESCs was then evaluated by manipulating the surrounding microniche upon which cells were delivered. Because pluripotent cells can respond to BMPs, scaffolds were constructed from hydroxyapatite-coated poly-L-lactic acid engineered to release BMP-2 (HA-PLGA + BMP-2) (18). One-million h-iPSCs or h-ESCs were seeded onto this microniche and placed into the context of a larger 4-mm critical-sized calvarial defect macroniche. These critical-sized defects do not spontaneously heal and any significant bone regeneration observed is a direct result of treatment (19). We hypothesized that by placing pluripotent cells in such an environment, robust osteogenesis could be stimulated and selected. Immunostaining of the regenerate was performed 7 d after implantation. The most intense staining for pSmad1 was appreciated in defects treated with h-iPSCs or h-ESCs seeded onto HA-PLGA + BMP-2 (Fig. 2*A*, *Top*, fourth and sixth box). Noticeably less staining was observed when cells were seeded onto HA-PLGA alone or when no cells were seeded at all (Fig. 2*A*, *top*, third and fifth box, and second box, respectively). Similar findings were appreciated for RUNX-2 and OCN, with the greatest staining demonstrated from pluripotent cells seeded on HA-PLGA + BMP-2 (Fig. 2*A*, *Middle* and *Bottom*, respectively). These findings therefore suggest greater in vivo osteogenic differentiation for h-iPSCs and h-ESCs in response to a BMP-2–releasing microniche compared with the standard HA-PLGA scaffold.

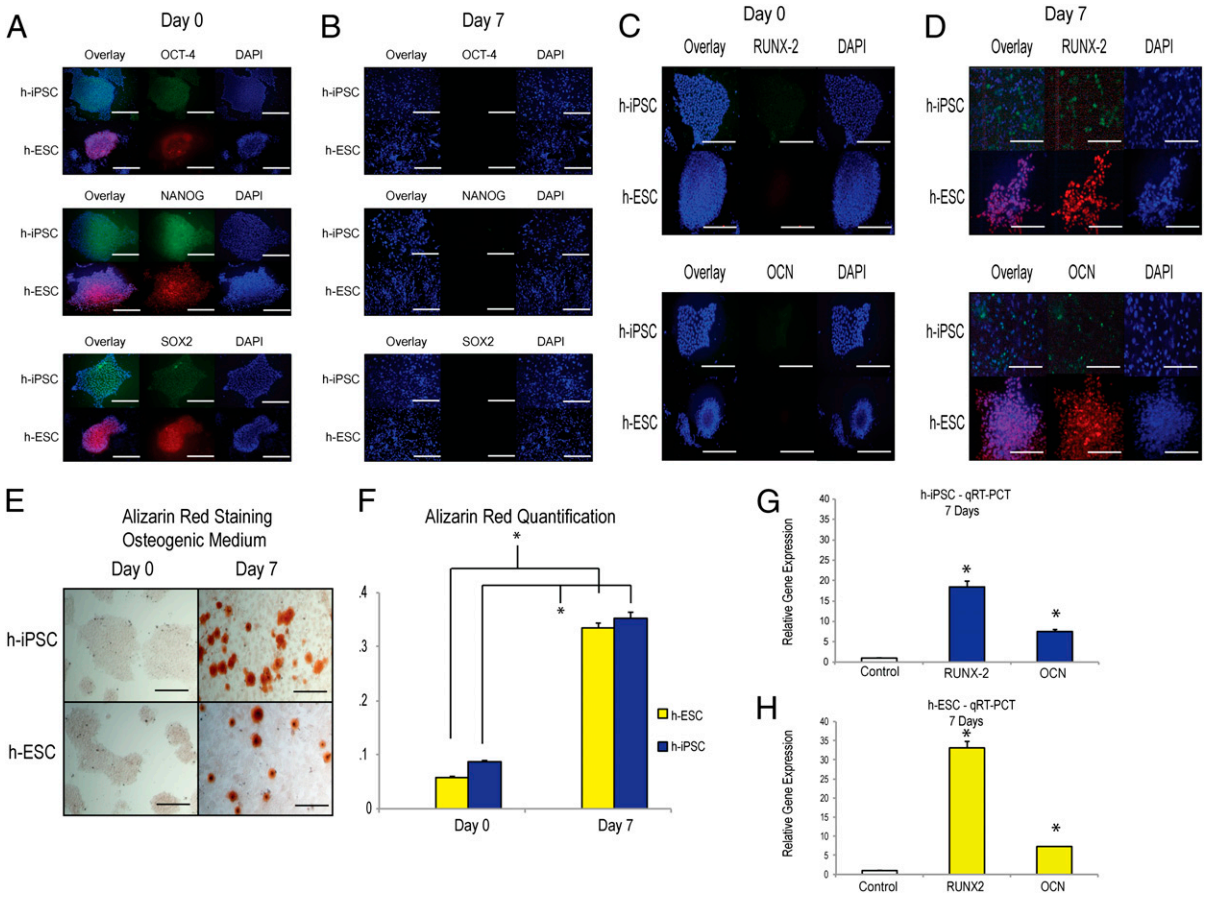

Fig. 1. Osteogenic differentiation medium stimulates in vitro osteogenic differentiation of pluripotent cells. (*A*) Immunofluorescent staining for OCT-4, NANOG, and SOX-2 for h-iPSCs (*Top*) and h-ESCs (*Bottom*) before treatment with ODM and (*B*) after 7 d of culture in ODM. (*C*) Immunofluorescent staining for RUNX-2 and OCN before treatment with ODM and (*D*) after 7 d of culture in ODM. (Scale bars, 50 μm.) (*E*) Alizarin red staining of h-iPSCs and h-ESCs before and after 7 d in ODM with (*F*) spectrophotometric quantification at both time points. (Scale bars, 75 μm.) (*G*) quantitative real-time PCR analysis of gene transcripts for RUNX-2 and OCN in h-iPSCs and (*H*) h-ESCs ($^*P < 0.05$).

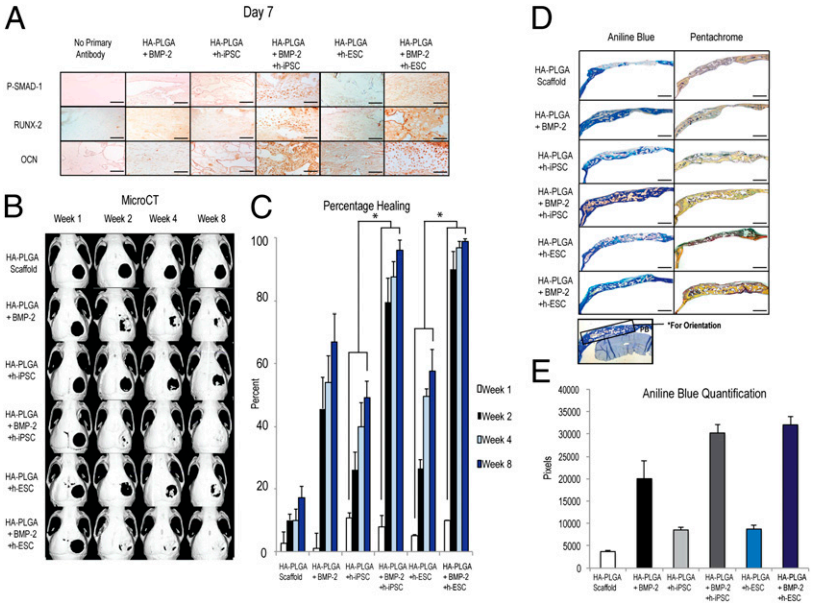

Fig. 2. In vivo bone regeneration by pluripotent cells. (*A*) Immunohistochemistry staining for pSmad1 (*Top*), RUNX-2 (*Middle*), and OCN (*Bottom*) 7 d after treatment of critical-sized calvarial defects with: (*i*) no antibody control, (*ii*) HA-PLGA + BMP-2 scaffold alone, (*iii*) HA-PLGA with h-iPSCs, (*iv*) HA-PLGA + BMP-2 with h-iPSCs, (*v*) HA-PLGA with h-ESCs, and (*vi*) HA-PLGA + BMP-2 with h-ESCs. (Scale bars, 100 μm.) (*B*) Representative microCT images of the regenerate at 1, 2, 4, and 8 wk after injury and treatment. Treatment groups included: (*i*) HA-PLGA scaffold alone, (*ii*) HA-PLGA + BMP-2 scaffold alone, (*iii*) HA-PLGA with h-iPSCs, (*iv*) HA-PLGA + BMP-2 with h-iPSCs, (*v*) HA-PLGA with h-ESCs, and (*vi*) HA-PLGA + BMP-2 with h-ESCs. (*C*) Quantification of percent healing in the region of the defect at 1, 2, 4, and 8 wk following injury (*$P < 0.05$ for each respective time point). (*D*) Aniline blue (*Left*) and pentachrome staining (*Right*) of regenerates at 8 wk. For orientation, the lower panel highlights region of interest in the box. PB, parietal bone. (Scale bars, 1 mm.) (*E*) Quantification of Aniline blue staining demonstrating total amount of osteoid in the defect.

Pluripotent markers were also evaluated by immunofluorescent staining of in vivo regenerates at 5 and 14 d following cellular implantation. Although OCT-4, NANOG, SOX-2, SSEA-4, TRA-1-60, and TRA-1-81 could all be detected at 5 d in the region of the regenerate, these markers could no longer be detected at 14 d when h-iPSCs or h-ESCs were seeded on HA-PLGA (Fig. S3) (15). In contrast, these same markers were much more difficult to detect at either 5 or 14 d when pluripotent cells were seeded onto HA-PLGA + BMP-2, suggesting incorporation of BMP-2 into the microniche accelerates loss of pluripotency by both h-iPSCs and h-ESCs in vivo (Fig. S3).

Given the observed enhanced expression of osteogenic markers in concert with down-regulation of pluripotent genes in response to HA-PLGA + BMP-2, we next determined the capacity for h-iPSCs and h-ESCs to promote in vivo bone regeneration. MicroCT scans performed on skeletal defects treated with HA-PLGA alone demonstrated minimal healing (Fig. 2*B*, first row, and Fig. 2*C*), and h-iPSCs seeded onto this same scaffold resulted in 49% regeneration by 8 wk (Fig. 2*B*, third row, and Fig. 2*C*). Using a more potent osteogenic microenvironment, HA-PLGA + BMP-2 scaffolds alone were capable of inducing 67% healing at 8 wk (Fig. 2*B*, second row, and Fig. 2*C*). This result was likely secondary to BMP-2 stimulation of endogenous cells surrounding the skeletal macroniche. h-iPSCs seeded onto HA-PLGA + BMP-2 resulted in the greatest amount of bone regeneration, with robust healing seen as early as 2 wk and complete (96%) healing of the critical-sized defect at 8 wk (Fig. 2*B*, fourth row, and Fig. 2*C*; *$P < 0.05$ for each respective time point). Similar results were observed with h-ESCs, as bone regeneration from cells seeded onto HA-PLGA + BMP-2 (99% healing) far outpaced that observed when HA-PLGA was used (Fig. 2*B*, fifth and sixth rows, and Fig. 2*C*; *$P < 0.05$ for each respective time point). Therefore, the HA-PLGA + BMP-2 microniche placed within the larger context of a skeletal defect macroniche was highly effective at promoting in vivo pluripotent cell bone formation and repair of a critical-sized defect. Finally, treatment groups were followed out to 28 wk to confirm durability of our findings, with little to no change noted beyond 8 wk by microCT (Fig. S4).

Bone Formation by Pluripotent Cells Without Teratoma Formation. Histological analysis with aniline blue and pentachrome staining was performed on sections to evaluate the quality of the regenerate. Robust bone formation was best appreciated in defects treated with pluripotent cells seeded onto HA-PLGA + BMP-2 (Fig. 2 *D* and *E*). Importantly, significant bone overgrowth was not appreciated and no teratoma formation was observed when h-iPSCs were implanted onto HA-PLGA (0 of 15 animals) or HA-PLGA + BMP-2 (0 of 12 animals) (Table S1). With h-ESCs, only two teratomas were appreciated among sections from five animals with pluripotent cells seeded on HA-PLGA and 10 animals with HA-PLGA + BMP-2 (Table S1). This was not entirely unexpected given the potency and differentiability of the one-million h-ESCs implanted and known differences at the epigenomic level with h-iPSCs incurred during reprogramming and prolonged passage in vitro (20–24). Nonetheless, the incidence of teratoma formation in the context of an osteogenic microniche from both h-iPSCs and h-ESCs was only 2 of 42 animals.

Pluripotent Cells Directly Contribute to in Vivo Osteogenesis. To confirm contribution of implanted pluripotent cells to the bony regenerate, immunohistochemistry for human nuclear antigen was performed (Fig. 3 *A* and *B*). Among defects with h-iPSCs on HA-PLGA + BMP-2, many positively stained cells were appreciated in either the osteogenic stroma or in appositional osteoblastic arrangements along the surface of newly formed bone (Fig. 3*A*). Interestingly, osteoclasts and osteocytes were found to be of mouse origin, but more than half of the osteogenic cells were human. This finding may reflect BMP-2 stimulation of host mouse cells from the underlying dura mater. Similar findings were also appreciated with h-ESCs implanted on HA-PLGA + BMP-2, as human cells were readily appreciated within the regenerate (Fig. 3*B*). Immunofluorescent staining of the regenerate for human nuclear antigen and OCN demonstrated colocalization of these markers in defects treated with either h-iPSCs or h-ESCs seeded on HA-PLGA + BMP-2 (Fig. 3*C*, third and fourth rows, respectively). No staining for either protein was appreciated with HA-PLGA alone. Interestingly, at the late time point of 8 wk, no human cells could be detected in the regenerate. This finding, however, may be consistent with bone turnover by the above noted mouse-derived osteoclasts. Finally, microdissection of the regenerate was performed for PCR analysis using human specific osteogenic primers (Table S2). In defects treated with h-iPSCs on HA-PLGA + BMP-2, both hOCN and hRUNX-2 could be detected (Fig. 3*D*, *Lower*, third column);

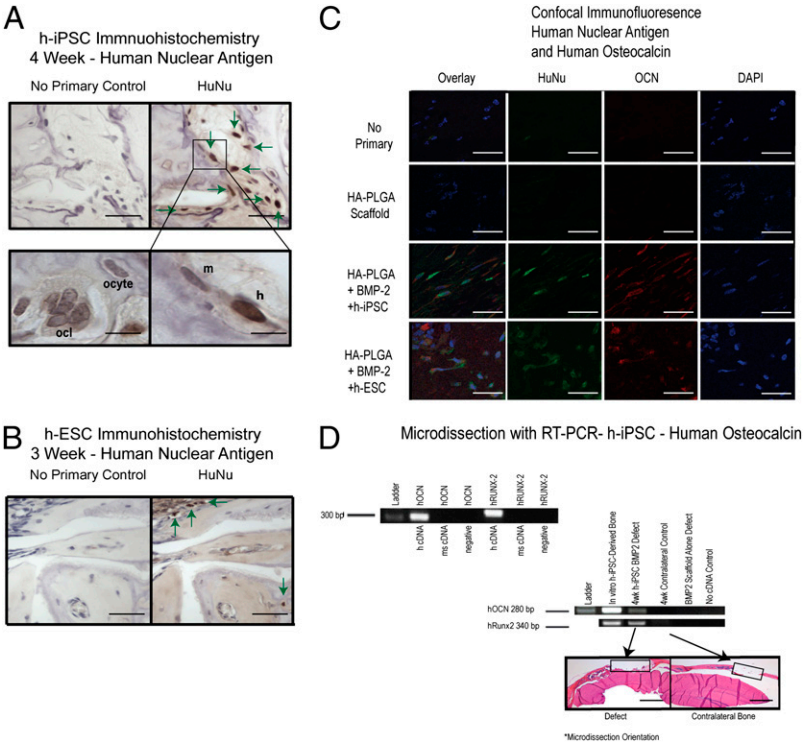

Fig. 3. Contribution of pluripotent cells to the bony regenerate. (*A*) Immunohistochemical stain for human nuclear antigen (HuNu) 4 wk after h-iPSC implantation. Note that human cell (h) in apposition to adjacent mouse osteoblast (m). Osteocytes (ocyte) and osteoclasts (ocl) did not stain for HuNu. (Scale bars, 35 μm for *Upper* photographs and 15 μm for *Lower* photographs.) (*B*) Immunohistochemical stain for HuNu three weeks after h-ESC implantation. Arrows show positively stained human-derived osteogenic cells. (Scale bars, 50 μm.) (*C*) Confocal microscopy of regenerate site 4 wk following h-iPSC implantation and 2 wk following h-ESC implantation. Immunofluorescent stain indicates cells positive for HuNu (green) in the nucleus and OCN (red) in cytosol. Rows: first row, no primary control; second row staining for HA-PLGA scaffold alone; third and fourth rows, h-iPSCs and h-ESCs with HA-PLGA + BMP-2 scaffold, respectively. (Scale bars, 25 μm.) (*D*) (*Upper*) Specificity of human primers for hOCN and hRUNX-2 using human and mouse cDNA samples. (*Lower*) PCR of microdissection samples from defect site at 4 wk. Dissected regions shown below in H&E stain, outlined in black boxes. Positive control provided by in vitro osteogenic differentiated h-iPSCs. hOCN and hRUNX-2 could be detected in regenerate from defects treated with h-iPSCs on HA-PLGA + BMP-2 scaffolds. Neither transcript was observed from contralateral uninjured mouse parietal bone or defects with HA-PLGA + BMP-2 scaffolds alone. (Scale bars, 2 mm.)

however, neither were observed when defects were treated with HA-PLGA + BMP-2 scaffolds alone (Fig. 3*D*, *Lower*, fifth column). Evaluation of the contralateral uninjured mouse parietal bone demonstrated absence of hOCN and hRUNX-2, confirming specificity of these primers for human transcripts (Fig. 3*D*, *Lower*, fourth column). Collectively, these data therefore strongly suggest that pluripotent cells placed onto a HA-PLGA + BMP-2 microniche within the larger context of a skeletal defect macroniche are capable of contributing to new bone formation with a greatly reduced propensity to form teratoma in vivo.

Extraskeletal Bone Induction by Osteogenic Microniche. To evaluate the capacity for HA-PLGA + BMP-2 scaffolds to guide in vivo osteogenic differentiation of pluripotent cells irrespective of macroenvironmental cues, extraskeletal subcutaneous implantation of h-iPSC and h-ESC on HA-PLGA + BMP-2 was performed. Histological analysis 8 wk later revealed de novo bone formation by both pluripotent cell types (three of seven animals, h-iPSC; three of four animals, h-ESC) (Fig. 4*A* and Table S1). Furthermore, immunofluorescent staining for both human nuclear antigen and OCN demonstrated colocalization and human nuclear antigen could be detected in the region of new bone by immunohistochemistry (Fig. 4 *B* and *C*). In contrast, no bone was observed when pluripotent cells were implanted on HA-PLGA alone, underscoring the inability for the extraskeletal macroniche to promote bone formation by implanted cells (Table S1). Thus, using multiple modalities, we have demonstrated that a strongly osteogenic microniche (HA-PLGA + BMP-2) is sufficient to guide bone formation by pluripotent cells in an in vivo extraskeletal macroenvironment.

Discussion

These findings reveal that acquisition of terminal cell fate by directly implanted pluripotent cells may be guided by local in vivo cues provided by the surrounding niche. In the setting of our strong osteogenic microniche placed within the context of a larger skeletal macroniche, h-iPSCs and h-ESCs were observed to undergo full differentiation and functional integration into newly forming bone regenerate. Surprisingly, this effect was so dominant that placement into such an environment of one-million pluripotent cells resulted in a very low frequency of teratoma formation. To our knowledge, this finding represents a unique demonstration of a direct effect from the surrounding, albeit artificial niche on implanted pluripotent cells, guiding in vivo engraftment and formation of bone in a meaningful manner.

Of note, the ability for in vivo induction of hESCs has been demonstrated with urogenital sinus and seminal vesicle mesenchyme, as such a heterospecific tissue recombination approach has been shown to be capable of directing small pluripotent cell aggregates to prostate-like tissue (25). However, Taylor et al. used far fewer cells (1×10^3) per construct, demonstrating expression of prostate specific antigen and other glandular epithelial markers only on a microscopic scale (25). Furthermore, use of such few cells would not be expected to typically yield teratoma formation (9). Alternatively, LeBleu et al. have shown the functional incorporation of h-ESCs into the kidney of a *Col4A3* knockout mouse model of Alport syndrome following intravascular injection of one-million pluripotent cells (26). Although histological improvement in glomerular basement membrane and ultimate kidney function was observed, no evaluation of teratoma formation was provided (26). Importantly, such an approach for cellular delivery has been shown to result in prolonged localization of ESCs to the spleen and lung and observation of teratoma development (27).

Recent studies have also evaluated the utility of pluripotent cells in bone regenerative strategies (28–30). In all of these reports, however, an extended period of ex vivo culture was required before implantation of constructs (28–30). Although some have reported a reduction in teratoma formation, each of these investigations have required in vitro predifferentiation of h-ESCs into mesenchymal cells before seeding onto osteoconductive scaffolds for in vivo bone formation (30). These studies therefore serve to underscore the significance of our findings as we were able to demonstrate formation and functional integration of de novo bone from direct placement of

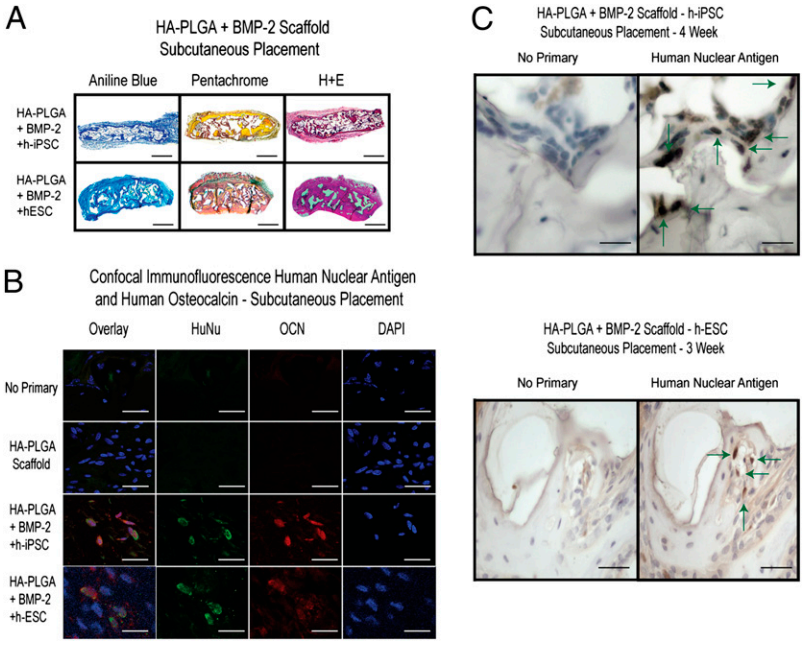

Fig. 4. Extraskeletal bone formation by pluripotent cells. (*A*) Aniline blue, pentachrome, and H&E stains 8 wk after subcutaneous implantation of h-iPSCs and h-ESCs on HA-PLGA + BMP-2. (Scale bars, 1 mm.) (*B*) Confocal microscopy showing colocalization of human nuclear antigen (HuNu) in green with OCN (red) for h-iPSCs on HA-PLGA + BMP-2 at 4 wk (third row) and h-ESCs on HA-PLGA + BMP-2 at 2 wk (fourth row). (Scale bars, 25 μm.) (*C*) Immunohistochemical human nuclear antigen stain following subcutaneous implantation of h-iPSCs at 4 wk (*Upper*) and h-ESCs (*Lower*) on HA-PLGA + BMP-2 scaffolds at 3 wk. Arrows demonstrate positively stained human-derived cells adjacent to de novo bone. (Scale bars, 25 μm for *Upper* h-iPSC photographs and 35 μm for *Lower* h-ESC photographs.)

pluripotent cells into skeletal defects. Furthermore, the ability to minimize teratoma formation emphasizes the critical role of the local environmental niche in guiding differentiation of implanted stem cells. Despite delivery of one-million pluripotent cells, our highly osteogenic microniche, in the context of a larger skeletal defect macroniche, was capable of directing acquisition of cell fate while simultaneously mitigating teratoma risk.

Using our model, we noted direct contribution of implanted pluripotent cells to the early bony regenerate in skeletal defects. However, the presence of human-derived cells at later time points could not be demonstrated. Despite this inability, stable bone formation was observed out to 28 wk, and the loss of implanted human cells was likely secondary to bone turnover. Bone formation and bone resorption are tightly coupled processes, and circulating mouse-derived osteoclasts may have been stimulated by either pluripotent cells themselves or by the BMP-2 releasing microniche (31, 32). It can also be argued that either the implanted cells or the HA-PLGA + BMP-2 scaffold may have also promoted long-term viability of host osteoblasts through enhanced vascularity. Multiple studies have shown h-iPSCs and BMP-2 to promote revascularization of ischemic wounds and upregulation of various angiogenic genes (33–35).

Nevertheless, the unique model used in this present work for directed differentiation (or selective amplification of subsets) of pluripotent cells represents significant progress in our understanding of the interplay between implanted cells and their surrounding niche. The acquisition of terminal cell fate by pluripotent cells in the in vivo setting may thus be coaxed from complex spatiotemporal signals and physical interaction with a specific endogenous environment that help to mediate functional tissue regeneration. Additional work still needs to be done, though, to precisely characterize what each of these signals and interactions are. Furthermore, although we have demonstrated this finding in the context of a bone-promoting niche, other tissue regeneration paradigms would benefit from a similar characterization of niche–stem cell interactions. Finally, from a therapeutic standpoint, the potential exists to fabricate alternative biomimetic scaffolds capable of directing differentiation of h-iPSCs or h-ESCs not just to bone, but also to cartilage, fat, nerve, muscle, glandular tissue, and so forth, yet simultaneously avoid teratoma formation (36, 37). Promising results have already been obtained using various nanomaterial scaffolds to craft specific niches supportive of both short-term cellular adhesion and proliferation, as well as longer-term viability, lineage differentiation, and functionalization (38, 39). Application of these unique biomimetic scaffolds to regenerative strategies using pluripotent cells may allow for the future development of innovative therapies to treat a wide range of diseases.

Materials and Methods

Cell Harvest and Derivation. Human adipose-derived stromal cells were isolated from the lipoaspirate of patients without medical comorbidities. Reprogramming to h-iPSCs was performed using a lentiviral vector (OCT-4, SOX-2, KLF-4, and c-MYC) and pluripotent characterization was performed by immunostaining for common h-ESC markers, pluripotency gene-expression analysis, and evaluation of promoter methylation status, as previously described (15). h-ESCs were derived from the H9 cell line (National Institutes of Health ID WA09).

Western Blot. Pluripotent cells were incubated in standard RIPA buffer with 0.5% phosphatase inhibitor and 0.5% protease inhibitor mixture mix (Sigma-Aldrich). Separation was performed on a NuPAGE Novex 4–12% Bis•Tris gel (Invitrogen) and membranes were probed with either monoclonal rabbit antiphospho-Smad1/5, anti-Smad5, or anti–α-tubulin antibodies in 1:1,000 dilution (Cell Signaling Technology). Detection was performed by enhanced chemiluminescence using the appropriate horse-radish peroxidase-linked secondary antibody (Jackson ImmunoResearch Laboratories).

Assessment of in Vitro Osteogenic Differentiation. Equal numbers of pluripotent cells were cultured on Matrigel in six-well plates. Cells were treated with mTeSR-1 or ODM (consisting of DMEM, 10% FBS, 100 μg/mL ascorbic acid, and 10 mM β-glycerophosphate) with or without rhBMP-2 (200 ng/mL). To evaluate marker expression, cells were trypsinized, resuspended in FACS buffer (2% FBS in PBS) and blocked before staining with fluorochrome-conjugated antibodies against SSEA-4 or RUNX-2 for flow cytometry. To evaluate osteogenesis, immunofluorescent staining was performed for OCT-4, NANOG, and SOX-2 at day 0 and day 7 of culture. Alizarin red staining was performed following 7 d of osteogenic differentiation, as previously described (40).

Kidney Capsule Injection. Evaluation of pluripotency through teratoma formation was assessed by injecting one-million h-iPSCs or h-ESCs beneath the kidney capsule of adult (60-d-old) Crl:NU(NCr)-*Foxn1*^{nu} CD-1 nude mice (Charles River) (16). All animals were cared for in accordance with approved protocols by the Institutional Animal Care and Use Committee at Stanford

University. After 8 wk, tumors were dissected and fixed. Parrafin embedded sections were stained with H&E.

Preparation and Seeding of Scaffolds. Hydroxyapatite-coated PLGA scaffolds were fabricated from 85 of 15 poly(lactic-coglycolic acid) by solvent casting and a particulate leaching process as previously described (41). For BMP-2–loaded scaffolds, 1.25 μg of recombinant human BMP-2 (rhBMP-2; Medtronic) was adsorbed onto fabricated scaffolds at a final concentration of 200 μg/mL and scaffolds were further lyophilized on a freeze drier overnight (Labconco). Scaffolds were seeded with one-million h-iPSCs or h-ESCs 8 h before implantation (42).

Creation of Skeletal Defects. Critical sized 4-mm skull defects were created in the right parietal skull bones of adult (60-d-old) male Crl:NU(NCr)-*Foxn1*^{nu} CD-1 nude mice. Scaffolds were seeded with one million h-iPSCs or h-ESCs 8 h before implantation (42). Animals were divided into six groups (n = minimum of five mice per group): (*i*) HA-PLGA scaffold without cells; (*ii*) HA-PLGA + BMP-2 scaffold without cells; (*iii*) HA-PLGA scaffold with h-iPSCs; (*iv*) HA-PLGA + BMP-2 scaffold with h-iPSCs; (*v*) HA-PLGA scaffold with h-ESCs; and (*vi*) HA-PLGA + BMP-2 scaffold with h-ESCs.

Subcutaneous Scaffold Placement. A 1-cm incision was made just over the inguinal fat pad of nude mice and a subcutaneous pocket was dissected. h-iPSCs and h-ESCs seeded HA-PLGA + BMP-2 scaffolds were placed under the skin just over this fat pad. Specimens were removed at four weeks for h-iPSCs and 3 wk for h-ESCs to evaluate bone formation.

Histological Staining. Human cells were positively stained with human specific anti-nuclear antigen antibodies (clone 235–1 mAB 1281; Millipore) using a mouse on mouse staining kit (Vector Laboratories) on 8-μm formalin-fixed paraffin-embedded tissue, according to the manufacturer's instructions. Immunohistochemistry and immunofluorescent staining were performed using Vectastain Elite kits (Vector Laboratories) on 8-μm formalin-fixed paraffin-embedded tissue according to the manufacturer's instructions. Immunohistochemistry was exposed using a biotinylated secondary antibody and DAB kit, and immunofluorescence was visualized with fluorescent secondary antibodies (Alexa Fluor; Invitrogen) on a confocal microscope. Aniline blue stain was carried out to stain collagen within bone tissue according to Masson's trichrome method. De novo bone was imaged with light microscopy and quantified with Adobe Photoshop CS5 (Adobe Systems) by pixel density. Pentachrome stain was carried out according to Movat's method.

In Vivo Imaging. Micro-CT was performed on live animals postoperatively (through 8-wk healing) using a high-resolution MicroCAT II (ImTek) imaging system (43). An in vivo imaging system was performed using the IVIS 200B imaging system. Luciferin (150 mg/kg in 200 μL) was injected into the peritoneal cavity and, after 10 min, the animals were placed into the imaging device. Images were acquired over 3 min (43).

ACKNOWLEDGMENTS. We thank Shane Morrison for his assistance with bioluminescent imaging; Divya Nag for her assistance with kidney capsule injection; Emily R. Nelson for her assistance with histological sectioning; Li Wang for his assistance with PCR experiments; and Andrew Lee for his assistance with pluripotent cell lines. This work was funded in part by National Institutes of Health (NIH) Grant 1F32AR057302-02 (to B.L.); NIH Grants 5U01HL099776, DP2OD004437, AG036142, and AI085575 (to J.C.W.); NIH Grants 1 R21 DE019274-01, RC2 DE020771-0, RC1 HL100490, 5U01HL099776, the Oak Foundation, California Institute for Regenerative Medicine Grant RL1-00662, and Hagey Laboratory for Pediatric Regenerative Medicine (to M.T.L.); and NIH Grants 5RC2DE20771-2, R01-HL058770, and the Stinehart/Reed awards (to I.L.W.).

1. Tsuji O, et al. (2010) Therapeutic potential of appropriately evaluated safe-induced pluripotent stem cells for spinal cord injury. *Proc Natl Acad Sci USA* 107(28):12704–12709.
2. Furth ME, Atala A (2009) Stem cell sources to treat diabetes. *J Cell Biochem* 106(4): 507–511.
3. Thomson JA, et al. (1998) Embryonic stem cell lines derived from human blastocysts. *Science* 282(5391):1145–1147.
4. Tiscornia G, Vivas EL, Izpisúa Belmonte JC (2011) Diseases in a dish: Modeling human genetic disorders using induced pluripotent cells. *Nat Med* 17(12):1570–1576.
5. Wernig M, et al. (2007) In vitro reprogramming of fibroblasts into a pluripotent ES-cell-like state. *Nature* 448(7151):318–324.
6. Zhao T, Zhang ZN, Rong Z, Xu Y (2011) Immunogenicity of induced pluripotent stem cells. *Nature* 474(7350):212–215.
7. Apostolou E, Hochedlinger K (2011) Stem cells: iPS cells under attack. *Nature* 474 (7350):165–166.
8. Tang C, et al. (2011) An antibody against SSEA-5 glycan on human pluripotent stem cells enables removal of teratoma-forming cells. *Nat Biotechnol* 29(9):829–834.
9. Miura K, et al. (2009) Variation in the safety of induced pluripotent stem cell lines. *Nat Biotechnol* 27(8):743–745.
10. Cao F, et al. (2007) Molecular imaging of embryonic stem cell misbehavior and suicide gene ablation. *Cloning Stem Cells* 9(1):107–117.
11. Moore KA, Lemischka IR (2006) Stem cells and their niches. *Science* 311(5769): 1880–1885.
12. Yu P, Pan G, Yu J, Thomson JA (2011) FGF2 sustains NANOG and switches the outcome of BMP4-induced human embryonic stem cell differentiation. *Cell Stem Cell* 8(3):326–334.
13. Xu RH, et al. (2002) BMP4 initiates human embryonic stem cell differentiation to trophoblast. *Nat Biotechnol* 20(12):1261–1264.
14. Xu RH, et al. (2005) Basic FGF and suppression of BMP signaling sustain undifferentiated proliferation of human ES cells. *Nat Methods* 2(3):185–190.
15. Sun N, et al. (2009) Feeder-free derivation of induced pluripotent stem cells from adult human adipose stem cells. *Proc Natl Acad Sci USA* 106(37):15720–15725.
16. Wesselschmidt RL (2011) The teratoma assay: An in vivo assessment of pluripotency. *Methods Mol Biol* 767:231–241.
17. Su W, et al. (2011) Bioluminescence reporter gene imaging characterize human embryonic stem cell-derived teratoma formation. *J Cell Biochem* 112(3):840–848.
18. Kim S, et al. (2008) In vivo bone formation from human embryonic stem cell-derived osteogenic cells in poly(d,l-lactic-co-glycolic acid)/hydroxyapatite composite scaffolds. *Biomaterials* 29(8):1043–1053.
19. Cowan CM, et al. (2004) Adipose-derived adult stromal cells heal critical-size mouse calvarial defects. *Nat Biotechnol* 22(5):560–567.
20. Phanstiel DH, et al. (2011) Proteomic and phosphoproteomic comparison of human ES and iPS cells. *Nat Methods* 8(10):821–827.
21. Takahashi K, et al. (2007) Induction of pluripotent stem cells from adult human fibroblasts by defined factors. *Cell* 131(5):861–872.
22. Takahashi K, Yamanaka S (2006) Induction of pluripotent stem cells from mouse embryonic and adult fibroblast cultures by defined factors. *Cell* 126(4):663–676.
23. Nishino K, et al. (2011) DNA methylation dynamics in human induced pluripotent stem cells over time. *PLoS Genet* 7(5):e1002085.
24. Bilic J, Izpisua Belmonte JC (2012) Concise review: Induced pluripotent stem cells versus embryonic stem cells: Close enough or yet too far apart? *Stem Cells* 30(1):33–41.
25. Taylor RA, et al. (2006) Formation of human prostate tissue from embryonic stem cells. *Nat Methods* 3(3):179–181.
26. LeBleu V, et al. (2009) Stem cell therapies benefit Alport syndrome. *J Am Soc Nephrol* 20(11):2359–2370.
27. Huang NF, et al. (2010) Embryonic stem cell-derived endothelial cells engraft into the ischemic hindlimb and restore perfusion. *Arterioscler Thromb Vasc Biol* 30(5):984–991.
28. Kuznetsov SA, Cherman N, Robey PG (2011) In vivo bone formation by progeny of human embryonic stem cells. *Stem Cells Dev* 20(2):269–287.
29. Arpornmaeklong P, Brown SE, Wang Z, Krebsbach PH (2009) Phenotypic characterization, osteoblastic differentiation, and bone regeneration capacity of human embryonic stem cell-derived mesenchymal stem cells. *Stem Cells Dev* 18(7):955–968.
30. Marolt D, et al. (2012) Engineering bone tissue from human embryonic stem cells. *Proc Natl Acad Sci USA* 109(22):8705–8709.
31. Guihard P, et al. (2012) Induction of osteogenesis in mesenchymal stem cells by activated monocytes/macrophages depends on oncostatin M signaling. *Stem Cells* 30(4):762–772.
32. Zheng Y, et al. (2012) BMP2/7 heterodimer can modulate all cellular events of the in vitro RANKL-mediated osteoclastogenesis, respectively, in different dose patterns. *Tissue Eng Part A* 18(5-6):621–630.
33. Levi B, et al. (2012) Enhancement of human adipose-derived stromal cell angiogenesis through knockdown of a BMP-2 inhibitor. *Plast Reconstr Surg* 129(1):53–66.
34. Suzuki H, et al. (2010) Therapeutic angiogenesis by transplantation of induced pluripotent stem cell-derived Flk-1 positive cells. *BMC Cell Biol* 11:72.
35. Margariti A, et al. (2012) Direct reprogramming of fibroblasts into endothelial cells capable of angiogenesis and reendothelialization in tissue-engineered vessels. *Proc Natl Acad Sci USA* 109(34):13793–13798.
36. Nelson TJ, Martinez-Fernandez A, Terzic A (2010) Induced pluripotent stem cells: Developmental biology to regenerative medicine. *Nat Rev Cardiol* 7(12):700–710.
37. Pozzobon M, Ghionzoli M, De Coppi P (2010) ES, iPS, MSC, and AFS cells. Stem cells exploitation for Pediatric Surgery: Current research and perspective. *Pediatr Surg Int* 26(1):3–10.
38. Zhao C, Tan A, Pastorin G, Ho HK (2012) Nanomaterial scaffolds for stem cell proliferation and differentiation in tissue engineering. *Biotechnol Adv* (Aug):9.
39. Ku SH, Lee SH, Park CB (2012) Synergic effects of nanofiber alignment and electroactivity on myoblast differentiation. *Biomaterials* 33(26):6098–6104.
40. Wan DC, et al. (2006) Osteogenic differentiation of mouse adipose-derived adult stromal cells requires retinoic acid and bone morphogenetic protein receptor type IB signaling. *Proc Natl Acad Sci USA* 103(33):12335–12340.
41. Chou YF, Huang W, Dunn JC, Miller TA, Wu BM (2005) The effect of biomimetic apatite structure on osteoblast viability, proliferation, and gene expression. *Biomaterials* 26(3):285–295.
42. Levi B, et al. (2010) Human adipose derived stromal cells heal critical size mouse calvarial defects. *PLoS ONE* 5(6):e11177.
43. Levi B, et al. (2011) Studies in adipose-derived stromal cells: Migration and participation in repair of cranial injury after systemic injection. *Plast Reconstr Surg* 127(3): 1130–1140.